GEOFIZIKA VOL. 11 1994

Original scientific paper
UDC 534.2 + 550.34

Application of acoustic wave solution for the analysis of reverberation

J. P. Narayan and Avadh Ram

Department of Geophysics, Banaras Hindu University, Varanasi – 221005, India

Received 8 February 1994, in final form 4 October 1994

Finite difference method offers a versatile approach to numerical computation of synthetic seismograms for a given subsurface complex geological model. Numerical solution for the acoustic wave has been derived using the Lax-Wendroff scheme for an inhomogeneous medium and implemented for the modelling of localized areas in the offshore region. Numerical seismograms have been obtained to identify the singing effect for different model geometries. The effect of source-receivers position, water depth and the frequency of source on the reverberation is studied. The generation of ghost reflections and its effect on the amplitude of reflected waves as well as on multiples for different source-depth positions is studied. The grid dispersion effect on the reflected signal and the reverberation is discussed for high-frequency signals. The analysis of numerical seismograms indicates that the energy radiating from a point source and remaining completely within a water layer may not cause singing, whereas the energy reflected from the deeper horizons is responsible for the singing effect on the reflections.

Primjena rješenja za akustičke valove na analizu odjeka

Postupak konačnih razlika omogućuje raznovrstan pristup numeričkom računanju sintetičkih seizmograma za zadani geološki model. Koristeći Lax-Wendroffovu shemu za nehomogeno sredstvo izvedeno je numeričko rješenje za akustičke valove, koje je primijenjeno za modeliranje dijelova podmorja. Studiran je utjecaj položaja stanice i izvora, dubine vode i frekvencije izvora na odjeke. Također je razmotreno generiranje lažnih refleksija i njihov utjecaj na amplitudu jednostruko i višestruko reflektiranih valova. Utjecaj mrežne disperzije na reflektirani signal diskutiran je za visokofrekventne signale.

Introduction

The growing interest in the numerical seismic modelling has led to a wide proliferation of methods of varying degrees of intricacy, accuracy and implementation ease. Such efforts are spurred by the awareness that exact analytical solution to the elastic wave equation does not exist for most subsurface

configurations of exploration interest. The solution for realistic models may be obtained only by approximate means. Numerical solution of the scalar and elastic wave equations have greatly aided geophysicists in the modelling of seismic wave fields in complicated geologic media and hence enhanced the degree of geologic interpretation. A method to solve the differential equations that govern seismic wave propagation in a complex geological medium numerically, has to be highly accurate and sensitive to subtle effects of the wave propagation. The method should allow coarse sampling and fast spatial fluctuations of medium properties for a large number of grids and propagation distances. Also, the method has to be well behaved at discontinuities of elastic parameters and should be fast. These methods include higher order schemes, central and one sided implicit as well as explicit methods, velocity stress schemes etc., as described by Alterman and Karal (1968), Boore (1972), Kelly et al. (1976), Virieux et al. (1984, 1986). Liu (1959) described wave propagation in a liquid layer for offshore seismic work. A fourth order MacCormack scheme has been given by Gottlieb and Turkel (1976). Alford et al. (1974) studied the accuracy of finite difference modelling of the acoustic wave equation. Yoon and McMechan (1992) have simulated a 3-D borehole environment to ensure the reliability of a numerical method for large impedance contrast. Vafidis et al. (1992) gave the modified Lax-Wendroff and MacCormack schemes which are more efficient than others. They have compared the numerical results with field data from an area containing a steam layer. The comparison showed the accuracy and stability of these schemes for a wide range of compressional and shear wave velocities.

Numerical solution for the acoustic wave is derived in this paper using the Lax-Wendroff scheme (Mitchell, 1969) for an inhomogeneous media. This is second order finite difference scheme in space and time. Acoustic wave solution is used for the modelling of localized offshore region. The effect of source-receivers position, water depth and the frequency of source on the reverberation are studied. The generation of ghost reflections and its effect on the amplitude of reflected signal as well as on multiples for different source-depth positions is discussed. The grid dispersion effect on the reflected signal as well as on the reverberations is given.

Solution of the acoustic wave equation

Let us assume a liquid medium which is two dimensional i.e. the density ρ and Lame's parameter λ depend only upon two coordinates, say x and z i.e. the displacements and stress component is independent of the third coordinate y. When a line source along the z axis acts on the medium, the equations of motion are reduced to

$$\rho \partial_{tt} u = \partial_x \tau_{xx} \tag{1}$$

$$\rho \partial_{tt} w = \partial_z \tau_{zz} \,, \tag{2}$$

and the Hooke's law takes the form,

$$\tau_{xx} = \tau_{zz} = \lambda(\partial_x u + \partial_z w). \tag{3}$$

Denoting the stress components as

$$\tau = \tau_{xx} = \tau_{zz} \,,$$

the equations (1), (2) and (3) can be written as:

$$\partial_t \dot{u} = 1/\rho \; \partial_x \tau \tag{4}$$

$$\partial_t \dot{w} = 1/\rho \; \partial_z \tau \tag{5}$$

and

$$\partial_t \tau = \lambda(\partial_x \dot{u} + \partial_z \dot{w}). \tag{6}$$

The equations (4), (5) and (6) can be brought into a first order hyperbolic partial differential equation,

$$\partial_t U = A \; \partial_x U + B \; \partial_z U \,, \tag{7}$$

where A and B are $n \times n$ real symmetric matrices and U is n component column vector:

$$U = \begin{bmatrix} \dot{u} \\ \dot{w} \\ \tau \end{bmatrix}, \quad A = \begin{bmatrix} 0 & 0 & \hat{\rho} \\ 0 & 0 & 0 \\ \lambda & 0 & 0 \end{bmatrix}, \quad B = \begin{bmatrix} 0 & 0 & 0 \\ 0 & 0 & \hat{\rho} \\ 0 & \lambda & 0 \end{bmatrix} \tag{8}$$

with $\hat{\rho} = 1/\rho$.

The equation (7) has been solved using the second order Lax-Wendroff scheme as follows (Mitchell, 1969):

$$\begin{aligned} U_{l,m}^{n+1} = \{ & I + p/2 \, A(\Delta_x + \nabla_{x)} + p/2 \, B(\Delta_z + \nabla_z) + p^2/4 \, [(A\Delta_x + B\Delta_z) + \\ & + (A\nabla_x + b\nabla_z) + (a\nabla_x + B\nabla_z) \, (A\Delta_x + B\Delta_z)\}] \, U_{l,m}^{n} \end{aligned} \tag{9}$$

where Δ_x and ∇_x are forward and backward difference operators respectively.

$$p = \Delta t / \Delta z = \Delta t / \Delta x = k / h \qquad \begin{aligned} \Delta_x A &= A(x+h) - A(x) \\ \nabla_x A &= A(x) - A(x-h) \end{aligned} \tag{10}$$

where Δt is the time step and Δx and Δz are the grid intervals in the x- and z-directions respectively.

Using the definitions in (10), the expression at right hand side of the scheme in (9) can be written as a linear combination of the unknown vector U at the time stage n, at the grid points making the schemes stencil. Unfortunately, this final expression can not be used because in order to get in a compact form the order of the products have been changed between A at some place and A or B at another place. The result is as follows:

$$\begin{aligned} U_{l,m}^{n+1} = & \{I - p^2/4\,[A_{l,m}\,(A_{l+1,m} + A_{l-1,m}) + B_{l,m}\,(B_{l,m+1} + B_{l,m-1}) + \\ & + 2(A_{l,m} + B_{l,m})\,(A_{l,m} + B_{l,m})]\}\; U_{l,m}^{n} + \{p/2\,A_{l,m} + \\ & + p^2/4\,[A_{l,m}\,(A_{l+1,m} + B_{l+1,m}) + (A_{l,m} + B_{l,m})\,A_{l,m}]\}U_{l+1,m}^{n} - \\ & - \{p/2\,A_{l,m} - p^2/4\,[A_{l,m}\,(A_{l-1,m} + B_{l-1,m}) + (A_{l,m} + B_{l,m})\,A_{l,m}]\}U_{l-1,m}^{n} + \\ & + \{p/2\,B_{l,m} + p^2/4\,[B_{l,m}\,(A_{l,m+1} + B_{l,m+1}) + (A_{l,m} + B_{l,m})\,B_{l,m}]\}U_{l,m+1}^{n} - \\ & - \{p/2\,B_{l,m} - p^2/4\,[B_{l,m}\,(A_{l,m-1} + B_{l,m-1}) + (A_{l,m} + B_{l,m})\,B_{l,m}]\}U_{l,m-1}^{n} - \\ & - p^2/4\,\{A_{l,m}B_{l+1,m} + B_{l,m}A_{l,m-1}\}\; U_{l+1,m-1}^{n} - \\ & - p^2/4\,\{A_{l,m}B_{l-1,m} + B_{l,m}A_{l,m+1}\}\; U_{l-1,m+1}^{n}\,. \end{aligned} \tag{11}$$

The matrices A and B are sparse, so all the matrix operations have been performed in equation (11) and used in the final expressions for the components of $U_{l,m}^{n+1}$.

The solution for the I term of the equation (11) is given as,

$$A_{l+1,m} + A_{l-1,m} = \begin{bmatrix} 0 & 0 & \hat{\rho}_{l+1,m} + \hat{\rho}_{l-1,m} \\ 0 & 0 & 0 \\ \lambda_{l+1,m} + \lambda_{l-1,m} & 0 & 0 \end{bmatrix}$$

$$B_{l,m+1} + B_{l,m-1} = \begin{bmatrix} 0 & 0 & 0 \\ 0 & 0 & \hat{\rho}_{l,m+1} + \hat{\rho}_{l,m-1} \\ 0 & \lambda_{l,m+1} + \lambda_{l,m-1} & 0 \end{bmatrix}$$

$$A_{l,m} + B_{l,m} = \begin{bmatrix} 0 & 0 & \hat{\rho}_{l,m} \\ 0 & 0 & \hat{\rho}_{l,m} \\ \lambda_{l,m} & \lambda_{l,m} & 0 \end{bmatrix}.$$

Hence,

$$A_{l,m}\,(A_{l+1,m}+A_{l-1,m})=\begin{bmatrix}0&0&\hat{\rho}_{l,m}\\0&0&0\\\lambda_{l,m}&0&0\end{bmatrix}\begin{bmatrix}0&0&\hat{\rho}_{l+1,m}+\hat{\rho}_{l-1,m}\\0&0&0\\\lambda_{l+1,m}+\lambda_{l-1,m}&0&0\end{bmatrix}=$$

$$=\begin{bmatrix}\hat{\rho}_{l,m}\,(\lambda_{l+1,m}+\lambda_{l-1,m})&0&0\\0&0&0\\0&0&\lambda_{l,m}\,(\hat{\rho}_{l+1,m}+\hat{\rho}_{l-1,m})\end{bmatrix}$$

$$B_{l,m}\,(B_{l,m+1}+B_{l,m-1})=\begin{bmatrix}0&0&0\\0&0&\hat{\rho}_{l,m}\\0&\lambda_{l,m}&0\end{bmatrix}\begin{bmatrix}0&0&0\\0&0&\hat{\rho}_{l,m+1}+\hat{\rho}_{l,m-1}\\0&\lambda_{l,m+1}+\lambda_{l,m-1}&0\end{bmatrix}=$$

$$=\begin{bmatrix}0&0&0\\0&\hat{\rho}_{l,m}\,(\lambda_{l,m+1}+\lambda_{l,m-1})&0\\0&0&\lambda_{l,m}\,(\hat{\rho}_{l,m+1}+\hat{\rho}_{l,m-1})\end{bmatrix}$$

$$(A_{l,m}+B_{l,m})\,(A_{l,m}+B_{l,m})=\begin{bmatrix}0&0&\hat{\rho}_{l,m}\\0&0&\hat{\rho}_{l,m}\\\lambda_{l,m}&\lambda_{l,m}&0\end{bmatrix}\begin{bmatrix}0&0&\hat{\rho}_{l,m}\\0&0&\hat{\rho}_{l,m}\\\lambda_{l,m}&\lambda_{l,m}&0\end{bmatrix}=$$

$$=\begin{bmatrix}\hat{\rho}_{l,m}\lambda_{l,m}&\hat{\rho}_{l,m}\lambda_{l,m}&0\\\hat{\rho}_{l,m}\lambda_{l,m}&\hat{\rho}_{l,m}\lambda_{l,m}&0\\0&0&\hat{\rho}_{l,m}\lambda_{l,m}\end{bmatrix}.$$

The first term $U^{(1)}$ of the right hand side of equation (11) is given by

$$U^{(1)}=\begin{bmatrix}1&0&0\\0&1&0\\0&0&1\end{bmatrix}-\frac{p^2}{4}\begin{bmatrix}\hat{\rho}_{l,m}\,(\lambda_{l+1,m}+\lambda_{l-1,m})&0&0\\0&0&0\\0&0&\lambda_{l,m}\,(\hat{\rho}_{l+1,m}+\hat{\rho}_{l-1,m})\end{bmatrix}+$$

$$+\begin{bmatrix}0&0&0\\0&\hat{\rho}_{l,m}\,(\lambda_{l,m+1}+\lambda_{l,m-1})&0\\0&0&\lambda_{l,m}\,(\hat{\rho}_{l,m+1}+\hat{\rho}_{l,m-1})\end{bmatrix}+$$

$$+2\begin{bmatrix}\hat{\rho}_{l,m}\lambda_{l,m}&\hat{\rho}_{l,m}\lambda_{l,m}&0\\\hat{\rho}_{l,m}\lambda_{l,m}&\hat{\rho}_{l,m}\lambda_{l,m}&0\\0&0&\hat{\rho}_{l,m}\lambda_{l,m}\end{bmatrix}\begin{bmatrix}\dot{u}^n_{l,m}\\\dot{w}^n_{l,m}\\\tau^n_{l,m}\end{bmatrix}.$$

The first values of $\dot{u}$, $\dot{w}$ and τ from the above relation are:

$$\dot{u}^{(1)} = \{1 - p^2/4\,[\hat{\rho}_{l,m}\,(\lambda_{l+1,m} + \lambda_{l-1,m}) + 2\hat{\rho}_{l,m}\,\lambda_{l,m})\,\dot{u}^n_{l,m} - p^2/2\,\hat{\rho}_{l,m}\,\lambda_{l,m}\,\dot{w}^n_{l,m}\}$$

$$\dot{w}^{(1)} = -p^2/2\,\hat{\rho}_{l,m}\,\lambda_{l,m}\,\dot{u}^n_{l,m} + \{1 - p^2/4\,[\hat{\rho}_{l,m}\,(\lambda_{l,m+1} + \lambda_{l,m-1}) + 2\hat{\rho}_{l,m}\,\lambda_{l,m}]\}\dot{w}^n_{l,m}$$

$$\tau^{(1)} = \{1 - p^2/4\,[\lambda_{l,m}\,(\hat{\rho}_{l+1,m} + \hat{\rho}_{l-1,m}) + \lambda_{l,m}\,(\hat{\rho}_{l,m+1} + \hat{\rho}_{l,m-1}) + 4\,\hat{\rho}_{l,m}\,\lambda_{l,m}]\}\,\tau^n_{l,m}\ .$$

After adding all the corresponding terms of equations (11) the components are finally given below:

$$\begin{aligned}\dot{u}^{n+1}_{l,m} = {} & \{1 - p^2/4\,[\hat{\rho}_{l,m}\,(\lambda_{l+1,m} + \lambda_{l-1,m} + 2\hat{\rho}_{l,m}\,\lambda_{l,m})\,\dot{u}^n_{l,m} - p^2/2\,\hat{\rho}_{l,m}\,\lambda_{l,m}\,\dot{w}^n_{l,m} + \\ & + p^2/4\,(\hat{\rho}_{l,m}\,\lambda_{l+1,m} + \hat{\rho}_{l,m}\,\lambda_{l,m})\,\dot{u}^n_{l+1,m} + p^2/4\hat{\rho}_{l,m}\,\lambda_{l+1,m}\,\dot{w}^n_{l+1,m} + p/2\,\hat{\rho}_{l,m}\,\tau^n_{l+1,m} - \\ & - \{-p^2/4\,(\hat{\rho}_{l,m}\,\lambda_{l-1,m} + \hat{\rho}_{l,m}\,\lambda_{l,m})\,\dot{u}^n_{l-1,m} - p^2/4\,(\hat{\rho}_{l,m}\,\lambda_{l-1,m})\,\dot{w}^n_{l-1,m} + \\ & + p/2\,\hat{\rho}_{l,m}\,\tau^n_{l-1,m}\} + p^2/4\,\hat{\rho}_{l,m}\,\lambda_{l,m}\,\dot{w}^n_{l,m+1} + p^2/4\,\hat{\rho}_{l,m}\,\lambda_{l,m}\,\dot{w}^n_{l,m-1} - \\ & - p^2/4\,\hat{\rho}_{l,m}\,\lambda_{l+1,m}\,\dot{w}^n_{l+1,m-1} - p^2/4\,\hat{\rho}_{l,m}\,\lambda_{l-1,m}\,\dot{w}^n_{l-1,m+1}\end{aligned} \tag{12}$$

$$\begin{aligned}\dot{w}^{n+1}_{l,m} = {} & -p^2/2\hat{\rho}_{l,m}\,\lambda_{l,m} + \{1 - p^2/4\,[\hat{\rho}_{l,m}\,(\lambda_{l,m+1} + \lambda_{l,m-1}) + 2\hat{\rho}_{l,m}\,\lambda_{l,m}]\}\,\dot{w}^n_{l,m} + \\ & + p^2/4\,\hat{\rho}_{l,m}\,\lambda_{l,m}\,\dot{u}^n_{l+1,m} + p^2/4\,\hat{\rho}_{l,m}\,\lambda_{l,m}\dot{u}^n_{l-1,m} + p^2/4\,\hat{\rho}_{l,m}\,\lambda_{l,m+1}\dot{u}^n_{l,m+1} + \\ & + p^2/4(\hat{\rho}_{l,m}\,\lambda_{l,m+1} + \hat{\rho}_{l,m}\,\lambda_{l,m})\,\dot{w}^n_{l,m+1} + p/2\,\hat{\rho}_{l,m}\,\tau^n_{l,m+1} - \\ & - \{p^2/4\,(\hat{\rho}_{l,m}\,\lambda_{l,m-1} + \hat{\rho}_{l,m}\,\lambda_{l,m})\,\dot{w}^n_{l,m-1} + p/2\,\hat{\rho}_{l,m}\,\tau^n_{l,m-1}\} - \\ & - p^2/4\,\hat{\rho}_{l,m}\,\lambda_{l,m-1}\,\dot{u}^n_{l-1,m-1} - p^2/4\,\hat{\rho}_{l,m}\,\lambda_{l,m+1}\,\dot{u}^n_{l-1,m+1}\end{aligned} \tag{13}$$

$$\begin{aligned}\tau^n_{l,m} = {} & \{1 - p^2/4\,[\lambda_{l,m}\,(\hat{\rho}_{l+1,m} + \hat{\rho}_{l-1,m}) + \lambda_{l,m}\,(\hat{\rho}_{l,m+1} + \hat{\rho}_{l,m-1}) + 4\,\hat{\rho}_{l,m}\,\lambda_{l,m}]\}\tau^n_{l,m} + \\ & + p/2\,\lambda_{l,m}\,\dot{u}^n_{l+1,m} + p^2/4\,\hat{\rho}_{l+1,m}\,\lambda_{l,m} + \hat{\rho}_{l,m}\,\lambda_{l,m})\,\tau^n_{l+1,m} - \\ & - \{p/2\,\lambda_{l,m}\,\dot{u}^n_{l-1,m} - p^2/4\,(\hat{\rho}_{l-1,m}\,\lambda_{l,m} + \hat{\rho}_{l,m}\,\lambda_{l,m})\,\tau^n_{l-1,m}\} + p/2\,\lambda_{l,m}\,\dot{w}^n_{l,m+1} + \\ & + p^2/4\,(\hat{\rho}_{l,m+1}\,\lambda_{l,m} + \hat{\rho}_{l,m}\,\lambda_{l,m})\,\tau^n_{l,m+1} - \{p/2\,\lambda_{l,m}\,\dot{w}^n_{l,m-1} - \\ & - p^2/4\,(\hat{\rho}_{l,m-1}\,\lambda_{l,m} + \hat{\rho}_{l,m}\,\lambda_{l,m})\}\tau^n_{l,m-1}\ .\end{aligned} \tag{14}$$

Source implementation and computational procedure

One of the important factors in forward modelling is the implementation of the source. Since, in two dimensional problem, an axial symmetry is implied, it is natural to utilize a line source. The solution of the two dimensional acoustic wave in a homogeneous infinitely extended medium with a line source is well known (Aki and Richards, 1980). Convolving the impulse response with the source excitation results in an integral which can be evaluated numerically. A Gaussian function whose frequency response is band limited with a known dominant frequency is assumed to define the source excitation. The line source with time delay of 0.015 s and its frequency spectrum are shown in Figures 1a and 1b. The investigated area has been

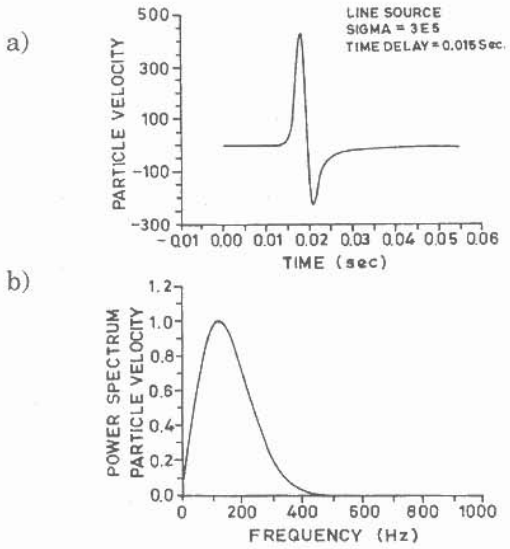

Figure 1. Line source (a) and its frequency spectrum (b) used in the modelling.

discretised into square grids of size 3 m and compressional velocities, densities and values of elastic constants of layers (Figures 2a and 2b) have been assigned to each grid point. The time step of 0.001 s has been used in the numerical computations. Then the source is inserted into the computational grid. This involves amplitude or pressure response specification, as well as the stress response specification. From these initial grids, the stress response has been computed for the next finite difference time step. For a second order algorithm, ten grids are involved at each time, for pressure response and stress component at the previous time step and at the current time step. For stability of the Lax-Wendroff formulation,

$$\alpha * \frac{k}{h} \leq \frac{1}{\sqrt{2}}$$

where k is the finite-difference time step, h is the grid increment in both x and z directions, α is the local compressional wave velocity.

Numerical results

The synthesized model is like an off-shore region with water depth ranging from 30 m to 105 m in a terrace form as shown in Figures 2a and 2b. The synthetic seismograms have been computed keeping the source and receivers at the surface (Figure 2a) as well as at depth (Figure 2b). The desired model has been discretised into square grids of size 3m and time step of 0.001 s has

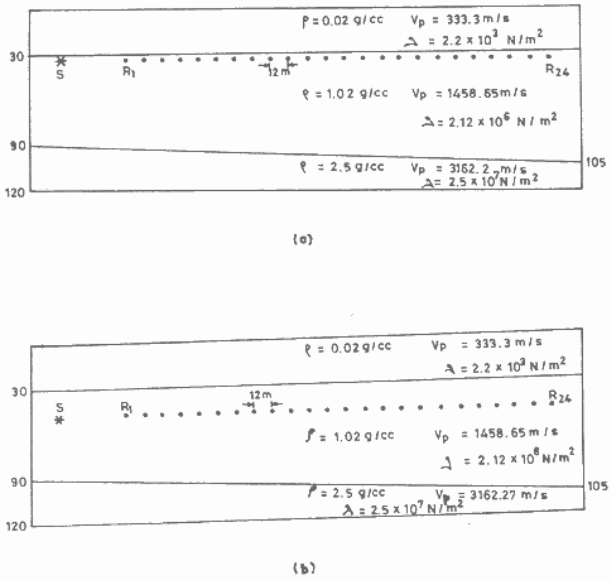

Figure 2. Model geometries of the off-shore region for numerical computations, (a) Source-receiver at the surface, (b) source-receiver at 18 m depth.

been taken in the computation. In order to avoid the large displacement in the source region, Alterman and Karal's method (1968) has been utilized. Two interfaces have been considered in the model, one between air and water and the other between water and oceanic bottom. The first medium, air, has density of 0.02 g/cm^3 and acoustic wave velocity 332.6 m/s. The second medium, water, has density of 1.02 g/cm^3 and the velocity of the acoustic wave is 1458.65 m/s. The bottom layer has a density of 2.5 g/cm^3 and the acoustic wave velocity is 3162.278 m/s.

Figure 2a shows the oceanic model with source-receiver position on the surface and Figure 2b depicts the model with the source-receiver position at a depth of 18 m. In these models, the air-water interface is at 30 m depth and the water-ocean bottom interface is sloping from 90 m to 105 m towards the west. The numerical seismograms have been computed keeping the receivers at 12 m interval. The pressure field has been recorded at 24 locations with source at an offset of 42 m from the first receiver. Figures 3 and 4 illustrate the numerically computed seismograms for the models shown in Figures 2a and 2b with a line source of frequency of 60 Hz. These seismograms reveal direct waves, reflected waves from the oceanic bottom as well as the multiples generated within the water layer. Since the reflector is dipping, the reverberation involves a slightly different position of the reflector than the primary and has a travel time slightly less than double the travel time of the primary. The latter fact permits to identify the reverberations by doubling the arrival time of primary reflections. The amplitude of the direct wave is decreasing very

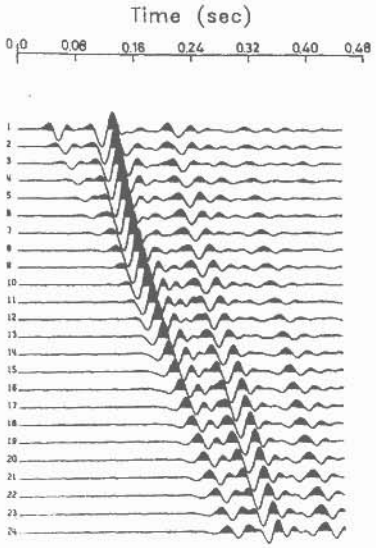

Figure 3. The pressure response of the offshore model as shown in Figure 2a for the acoustic wave of frequency of 60 Hz as a function of time.

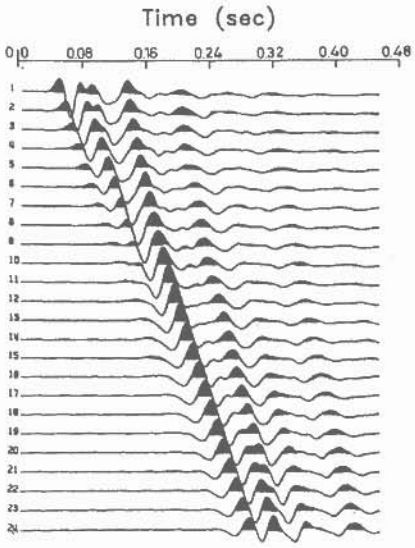

Figure 4. The pressure response of the offshore model shown in Figure 2b for the acoustic wave of frequency of 60 Hz as a function of time.

rapidly with the offset. From these figures, it may also be inferred that the amplitude of the direct wave is greater when the source and receivers are at 18 m depth, than when the source and receivers are at the surface. The rapid decrease of amplitude of the direct waves with offset in both cases indicates that the energy remaining in the water can not cause reverberation. The decrease of amplitude of the reflected waves with offset, in the case when the source and receiver points are at depth, is less than the decrease when the source and receivers are at the surface. When source and receivers are at depth, the amplitude of the singing is smaller compared to when the source and receivers are at the surface. The singings are not so clear in the second case due to the effect of interference of the ghost reflections and the reflected signals.

To examine the effect of water depth, the depth of each interface has been increased two times in both of the models. In these enlarged models, the depth of air-water interface is 60 m and the depth of the dipping oceanic bottom ranges from 180 m to 210 m. The grid size has been taken the same as in Figures 2a and 2b. Figures 5 and 6 show the numerical responses of the models for a line source having frequency of 45 Hz. The above figures also depict the similar waves i. e. direct waves, reflected waves and the multiples. However, the amplitude of the reflected wave as well as multiples are smaller

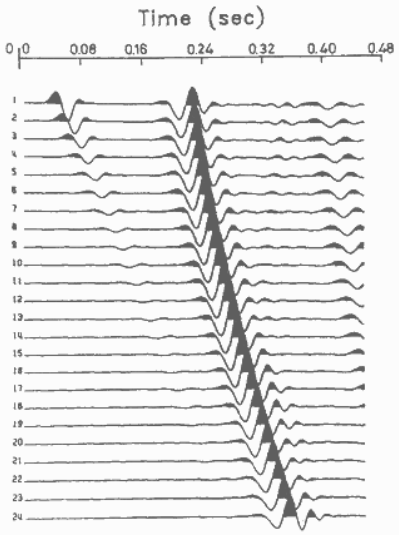

Figure 5. The pressure response of the offshore model with double depth of each interface shown in Figure 2a for the acoustic wave of frequency of 45 Hz.

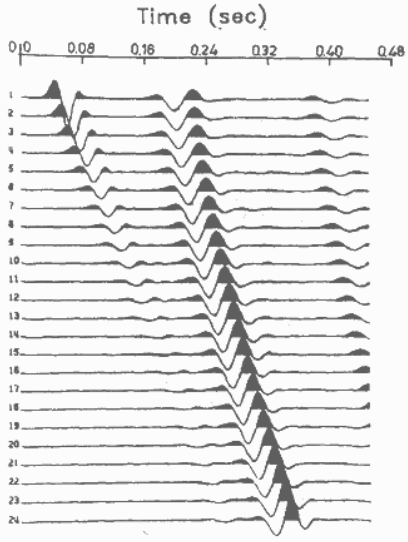

Figure 6. The pressure response of the offshore model with double depth of each interface shown in Figure 2b for the acoustic wave of frequency of 45 Hz.

as compared to the amplitude of the wave in Figures 3 and 4 due to the usual spreading effect. When the depth of the water layer is increased, the reverberations are more clear in both the cases i. e. when the source and receivers are at the surface and at depth. The interpretation of these seismograms shows that in this case also the amplitude of the reflected waves is increasing with offset, when source receivers are at depth. This may be due to the effect of wide angle phenomenon. The increase of amplitude of the multiples with offset in both the cases is similar.

When the source and receivers are at depth of 18 m, the effect of ghost reflections on the reflected signal and on the reverberation has been shown in Figures 4 and 6. A phase shift of 180°, equivalent to half a wavelength, occurs at additional reflection of ghost reflection and hence the effective path difference between the direct and the ghost reflection is $(\lambda/2 + 2d)$ where d is the depth of the source. Interference of the ghost reflection and the primary depends on the fraction of the wavelength represented by the difference in effective path length. Since seismic wavelet is made up of a range of frequencies, the interference effect will vary for the different components. In these figures, the amplitude of the reflected wave is small for shorter offset, which may be due to the destructive interference of the ghost reflection and the primary. The increase in the amplitude with offset may be due to the con-

structive interference effect. Similarly, the amplitude of the multiples in these cases are small compared to the case where the source and receivers are at the surface, due to the interference effects (Figure 3 and Figure 5).

The numerical seismograms have also been computed to study the grid dispersion using the Lax-Wendroff scheme for different frequencies. In fact, the number of grid points per wavelength has been changed by taking different frequencies. Figures 5 and 6 illustrate the response of the model for a line source of frequency 45 Hz. In these cases, there are about 11 grids per wavelength. From these figures, it has been inferred that there is no grid dispersion. Similarly, the Figures 3 and 4 show the response of the model for a line source having dominant frequency of 60 Hz. In this case, there are about 8 grids per wavelength which is less than the required grids to eliminate the grid dispersion. There is very small grid dispersion as shown by these figures. The effect of grid dispersion has also been shown in the Figures 7 and 8 for both source-receiver positions. The frequency used in this case is 120 Hz and the grid size is the same as 3 m. In effect, there are only 4 grids per wavelength. Strong grid dispersion is present in both of the computed seismograms. After the primary reflection, the dispersion is so pronounced that it is very difficult to recognize the reverberations. It has also been inferred that the grid dispersion increases with the travel time.

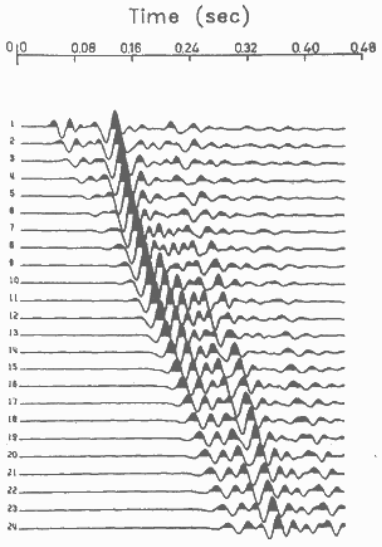

Figure 7. The pressure response of the offshore model shown in Figure 2a for the acoustic wave of frequency of 120 Hz.

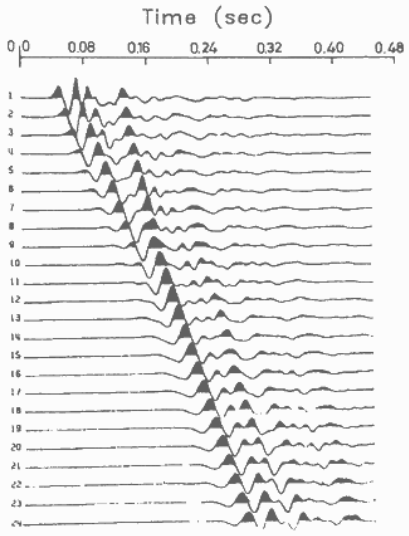

Figure 8. The pressure response of the offshore model shown in Figure 2b for the acoustic wave of frequency of 120 Hz.

Discussion and conclusions

Recently, a number of techniques have been pursued in an effort to improve the computational performance of the finite-difference solutions to the wave equations. These include higher-order schemes, central and one-sided implicit as well as explicit methods, velocity stress schemes etc., as described by Alterman and Karal (1968), Boore (1974), Kelly et al. (1976), Stephen (1983), George et al. (1987) and Tsingas et al. (1990). The modified Lax-Wendroff and MacCormack schemes given by Vafidis et al. (1992) are more efficient than other schemes for most of the modelling problems. Comparison of numerical results given by Vafidis et al. (1992) with the actual field record from a prospecting area containing steam layers, show that the Lax-Wendroff and MacCormack schemes are stable and accurate for a wide range of compressional to shear-wave velocity ratios. Yoon and McMechan (1992) have simulated a 3-D borehole environment to ensure the reliability of numerical method for large impedance contrast. The differential equation for the acoustic wave using the Lax-Wendroff scheme has been solved. This scheme is second order and accurate in both space and time. Liu (1959) has given the solution of the pressure wave equation for a point source in the water layer as well as transient amplitude response with depth and time. This solution indicated a too rapid decay of the energy *i.e.* about 80 db in 1.2 s. Backus (1959) has studied the nature of water reverberations and their elimination. The reverberations have similar waveform as the desired signal reflected from the deeper strata. Middleton and Whittlesey (1968) have given the seismic models and deterministic operator for marine reverberations. The numerically computed seismograms shown in Figures 3–8, illustrate that the amplitude of the direct wave from source to receivers decreases very rapidly with offset. It has been concluded from the numerical seismograms that the energy remaining completely in water can not cause reverberation. This result corroborates with the previous work (Liu, 1959; Backus, 1968). Stephen (1983) compared the finite-difference and reflectivity synthetic seismograms for laterally homogeneous sea floor models with step and ramp discontinuities in the elastic properties. He found that for step discontinuity, *i.e.* for large impedance contrast, the simple central difference scheme is not stable. For ramp discontinuity the scheme was stable. With this scheme such type of a problem does not arise. The generation of the reverberation has been explained by the elementary acoustic theory. For convenience, it has been referred as extended source solution. The deeper reflections from the oceanic bottom can be represented sufficiently accurately as a plane wave parallel to the ocean floor. Transient solution shows that the upward traveling wave proceeds to the surface, reflected with a polarity reversal, travels downward to the bottom and again partially reflected according to the conventional reflection coefficient formula. This process is repeated several times until the energy decreases to zero. It has been obtained that for greater source-receivers depth position, the amplitude of the reverberation is less as

compared to shallow source-receivers positions due to the destructive interference (Figures 5 and 6). It should not come as a surprise to learn that in spite of its limitations (in terms of grid dispersion and stability) the scheme has given good response for the models.

Acknowledgement – One of us (J. P. N.) is thankful to the University Grant Commission, New Delhi, for the Fellowship under the DRS programme of the Department.

References

Aki, K. and P. Richards (1980): Quantitative seismology, theory and methods, V. I., W. H. Freeman and Co, San Francisco.

Alford, R. M., Kelly, K. R. and D. M. Boore (1974): Accuracy of finite difference modelling of the acoustic wave equation, Geophysics, **39**, 834–842.

Alterman, Z. S. and F. C. Karal, Jr. (1968): Propagation of elastic waves in layered media by finite difference methods, Bull. Seism. Soc. Am., **58**, 367–398.

Backus, M. M. (1959): Water reverberations – their nature and elimination, Geophysics, **24**, 223–261.

Boore, D. M. (1972): Finite difference methods for seismic wave propagation in heterogeneous material, *in* Bolt, B. A. (Editor): Methods in Computational Physics, **11**, Academic Press Inc, New York.

George, Th., Virieux, J. and R. Madariaga (1987): Seismic wave synthesis by Gaussian beam summation: A comparison with finite difference, Geophysics, **52**, 1065–1073.

Gottlieb, D. and E. Turkel (1976): Dissipative two–four methods for time dependent problems, Math. Comp., **30**, 703–723.

Karal, F. C. and J. B. Keller (1959): Elastic wave propagation in homogeneous and inhomogeneous media, J. Acoust. Soc. Am., **31**, 694–705.

Kelly, K. R., Ward, R. W., Treitel, S. and R. M. Alford (1976): Synthetic seismograms: A finite-difference approach, Geophysics, **41**, 2–27.

Liu, D. T., (1969): Wave propagation in liquid layer, Geophysics, *24*, 658–666.

Middleton, D. and J. Rb. Whittlesey (1968): Seismic models and deterministic operators for marine reverberation, Geophysics, **33**, 557–583.

Mitchell, A. R. (1969): Computational methods in partial difference equations, John Wiley & Sons, New York.

Stephen, R. A. (1983): A comparison of finite difference and reflectivity seismograms for marine models, Geophys, J. R. astr. Soc., **72**, 39–58.

Tsingas, C., Vafidis, A. and E. R. Kanasewich (1990): Elastic wave propagation in transversely isotropic media using finite difference, Geophys. Prosp., **30**, 933–949.

Vafidis, A., Abramovici, F. and E. R. Kanasewich (1992): Elastic wave propagation using fully vectorized high order finite difference algorithms, Geophysics, **57**, 218–232.

Virieux, J. (1984): SH-wave propagation in heterogeneous media: Velocity-stress finite-difference method, Geophysics, **49**, 1933–1957.

Virieux, J. (1986): P-SV wave propagation in heterogeneous media: Velocity-stress finite-difference method, Geophysics, **51**, 889–901.

Yoon, K. H. and G. A. McMechan (1992): 3-D finite-difference modelling of elastic waves in bore hole environments, Geophysics, **57**, 793–804.

Correspondig author's address: J. P. Narayan, Department of Geophysics, Banaras Hindu University, Varanasi – 221005, India